

Few-body perspective of quantum anomaly in two-dimensional Fermi gases

X. Y. Yin,¹ Hui Hu,¹ and Xia-Ji Liu¹

¹Centre for Quantum and Optical Science, Swinburne University of Technology, Melbourne, Victoria 3122, Australia

(Dated: January 10, 2020)

Quantum anomaly manifests itself in the deviation of breathing mode frequency from the scale invariant value of 2ω in two-dimensional harmonically trapped Fermi gases, where ω is the trapping frequency. Its recent experimental observation with cold-atoms reveals an unexpected role played by the effective range of interactions, which requires quantitative theoretical understanding. Here we provide accurate, benchmark results on quantum anomaly from a few-body perspective. We consider the breathing mode of a few trapped interacting fermions in two dimensions up to six particles and present the mode frequency as a function of scattering length for a wide range of effective range. We show that the maximum quantum anomaly gradually reduces as effective range increases while the maximum position shifts towards the weak-coupling limit. We extrapolate our few-body results to the many-body limit and find a good agreement with the experimental measurements. Our results may also be directly applicable to a few-fermion system prepared in microtraps and optical tweezers.

Quantum anomaly arises if a certain symmetry of a classical theory (i.e., action) of the system fails to hold when a full quantum description is developed. One important example is the deviation from the scale invariant breathing mode frequency in two-dimensional (2D) ultracold atomic quantum gases [1, 2]. In a classic 2D gas interacting through zero-range interaction, a hidden $SO(2, 1)$ symmetry leads to an *exact* breathing mode frequency of $\omega_B = 2\omega$, where ω is the trapping frequency [1]. In a 2D quantum gas, the requirement of renormalization of the contact interaction leads to an additional length scale, the 2D scattering length. Therefore, the breathing mode frequency ω_B deviates from 2ω and depends on the scattering length. This is in contrast to the three-dimensional unitarily interacting quantum gas, where infinitely strong interaction strength leads to scale invariance and the preservation of $SO(2, 1)$ symmetry [3].

Experimental verification of quantum anomaly in 2D quantum gases comes with several interesting surprises. The initial idea of a weakly-interacting 2D Bose gas [1, 2] does not work since the breathing mode frequency shift is too small to be observable. A strongly interacting two-component 2D Fermi gas of ^{40}K and ^6Li atoms appears to be a better candidate [4–6]. However, the early observation of about 1% frequency shift from 2ω [7] is much smaller than the 10% anomaly predicted for zero-range contact interaction at zero temperature [4, 5]. This discrepancy is probably caused by the large temperature of the ^{40}K Fermi gas in the experiment [7], as suggested by virial expansion studies [8, 9]. In two most recent experiments with ^6Li atoms, the 2D Fermi gas was cooled down to one-tenth of Fermi temperature, to avoid any dominant finite temperature effect [10, 11]. Surprisingly, the measured quantum anomaly, about 2 – 3%, is still at the same level as in the first observation [7]. This unexpected, much reduced quantum anomaly is now understood as a result of a significant effective range of interactions induced by the tight axial confinement [12–14] that is necessary to restrict the motion of atoms into two

dimensions [12, 15]. An approximate many-body theory that takes into account Gaussian pair fluctuations (GPF) has then been developed, giving rise to a qualitative explanation for the experimental observation [13]. More accurate many-body calculations (except quantum Monte Carlo simulations [16–18]) are difficult to carry out at finite effective range, due to strong correlation inherent in 2D interacting Fermi gases.

In this Letter, we aim to provide benchmark predictions on quantum anomaly from a *few-body* perspective. Our purpose is three-fold. First, few-body systems can be solved exactly with high accuracy. Therefore, the few-body results include all correlations that can not be accounted for in the approximate mean-field and GPF studies. Here we use explicitly correlated Gaussian (ECG) basis set expansion approach [19, 20] to understand the breathing mode frequency in a small Fermi cloud with up to six particles. Second, few-body systems provide a bridge between the two-body physics and many-body physics. Many results in the many-body limit can be successfully deduced from few-body studies [21–26]. In this work, we find that our few-body results reveal two important features observed in the experiments in the presence of a nonzero effective range [10, 11]: the maximum quantum anomaly reduces gradually with increasing effective range while the peak position shifts to the weakly-interacting regime. Finally, it is worth emphasizing that the few-fermion system under consideration can nowadays be routinely prepared by using microtraps [27] or optical tweezer [28, 29]. Thus, the few-body result should be of its own interest and we anticipate that our few-body predictions with tunable number of particles might be directly examined in future experiments.

Model Hamiltonian. — We start by mentioning the s -wave scattering phase shift of two particles in 2D, which can be expanded in the low-energy limit as [30, 31]

$$\cot[\delta(k)] = \frac{2}{\pi} \left[\gamma + \ln \left(\frac{ka_{2D}}{2} \right) \right] + \frac{1}{2} k^2 R_s + \dots, \quad (1)$$

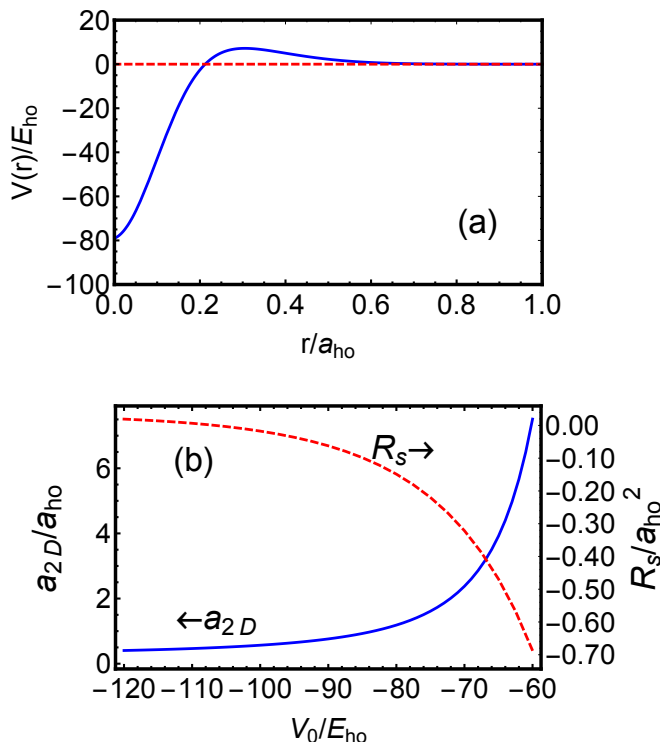


FIG. 1. (a) Pseudopotential $V(r)$ at $V_0/E_{\text{ho}} = -79.04$ and $r_0/a_{\text{ho}} = 0.104$. Here, $E_{\text{ho}} = \hbar\omega$ and $a_{\text{ho}} = \sqrt{\hbar/(m\omega)}$ are the energy and length of the harmonic oscillator, respectively. This potential coincides with the potential used in obtaining the third diamond symbol of Fig. 2(c). Dashed line marks the line $V(r) = 0$. (b) The 2D scattering length a_{2D} (solid line, scale on the left) and the effective range R_s (dashed line, scale on the right) as a function of potential depth V_0 at $r_0/a_{\text{ho}} = 0.1$.

where $\gamma \simeq 0.577$ is Euler's constant, a_{2D} the 2D scattering length and R_s the effective range [32]. R_s is related to the asymptotic form of the normalized scattering wave function $u(r)$ of a particular interaction potential by

$$R_s = 2 \int_0^\infty [\ln^2(r/a_{2D}) - u^2(r)] r dr. \quad (2)$$

In 2D, the scattering length a_{2D} is always positive. The two-component Fermi gas goes through a crossover from a Bose-Einstein condensate (BEC) to a Bardeen-Cooper-Schrieffer (BCS) superfluid as a_{2D} increases. However, unlike 3D, there is no scale invariant unitarity limit where the interaction strength diverges. Instead, the strongly interacting regime is around $\ln(k_F a_{2D}) = 0$, where k_F is the characteristic Fermi wavevector.

We consider a two-component Fermi gas consisting of N_\uparrow spin-up and N_\downarrow spin-down atoms ($N_\uparrow = N_\downarrow = N$) under harmonic confinement with transverse trapping frequency ω . The system Hamiltonian reads,

$$\mathcal{H} = \sum_\sigma \sum_{i_\sigma} \left[-\frac{\hbar^2 \nabla_{i_\sigma}^2}{2m} + \frac{m\omega^2 \vec{r}_{i_\sigma}^2}{2} \right] + \sum_{i_\uparrow, i_\downarrow} V(r_{i_\uparrow i_\downarrow}), \quad (3)$$

where m is the mass of a single atom, \vec{r}_{i_σ} ($i_\sigma = 1, \dots, N$ and $\sigma = \uparrow, \downarrow$) denotes the 2D position vector of the i th spin-up or down atom with respect to the trap center, and $V(r)$ is the interspecies two-body interaction potential that depends on the distance $r_{i_\uparrow i_\downarrow} \equiv |\vec{r}_{i_\uparrow} - \vec{r}_{i_\downarrow}|$.

The effective range R_s induced by a tight axial confinement in 2D Fermi gas experiments is negative [13]. To simulate a negative R_s , we employ a pseudopotential,

$$V(r) = V_0 \exp\left(-\frac{r^2}{2r_0^2}\right) - V_0 \frac{r}{a_{\text{ho}}} \exp\left[-\frac{r^2}{2(2r_0)^2}\right], \quad (4)$$

which is numerically amenable to ECG simulations. Alternative pseudopotential is also examined to check the negligible effects beyond effective range [33]. As exemplarily shown in Figure 1(a), the potential exhibits two features that are essential for supporting a shape resonance: an attractive well that supports virtual bound states and a potential barrier that couples the virtual bound state to the free-space scattering states [18]. Negative R_s becomes possible near a shape resonance. Figure 1(b) shows the 2D scattering length a_{2D} and effective range R_s as a function of the depth of potential V_0 for a fixed r_0 . As the depth of potential increases, both a_{2D} and the absolute value of R_s decreases until the next bound state appears. Another interesting feature of the potential is that the volume is positive, and therefore cannot support a two-body bound state when $V_0 \rightarrow 0$. Here, we restrict ourself to potential that supports at most one two-body bound state in free space. By adjusting both V_0 and r_0 , one can achieve a wide range of combination of a_{2D} and R_s . The limitation for our potential is that it is not possible to produce a small a_{2D} and large $|R_s|$ at the same time.

We solve the time-independent Schrödinger equation for the Hamiltonian given in Eq. (3) using ECG basis set expansion approach [19, 20, 33]. We expand the eigenstates of the Hamiltonian in terms of ECG basis functions, which depend on a number of nonlinear variational parameters that are optimized through energy minimization [20, 34–36]. After a proper basis set is constructed, we calculate various ground-state properties of a few-fermion system with number of particles $(N_\uparrow, N_\downarrow) = (1, 1), (2, 2)$ and $(3, 3)$. For a trapped system, it is convenient to use Fermi wavevector $k_F = \sqrt{2}(N_{\text{tot}})^{1/4} a_{\text{ho}}^{-1}$, which is basically the wavevector of a non-interacting Fermi gas at the trap center in the large-particle limit [15]. Here, $N_{\text{tot}} \equiv N_\uparrow + N_\downarrow$ is the total number of atoms and $a_{\text{ho}} = \sqrt{\hbar/(m\omega)}$ the harmonic oscillator length.

Breathing mode frequency. — The breathing mode of two-component Fermi gases is a density fluctuation excited by the perturbation $\mathcal{F} \propto \sum \vec{r}_{i_\sigma}^2$. It appears as a well-defined single mode in the density response function in the low-momentum and low-energy limit, i.e., $S_{\mathcal{F}}(\omega) \propto \delta(\omega - \omega_B)$. As a result, we may use a sum-rule approach to calculate the breathing mode frequency, $\omega_B^2 = m_{p+2}/m_p$, through the energy weighted moments

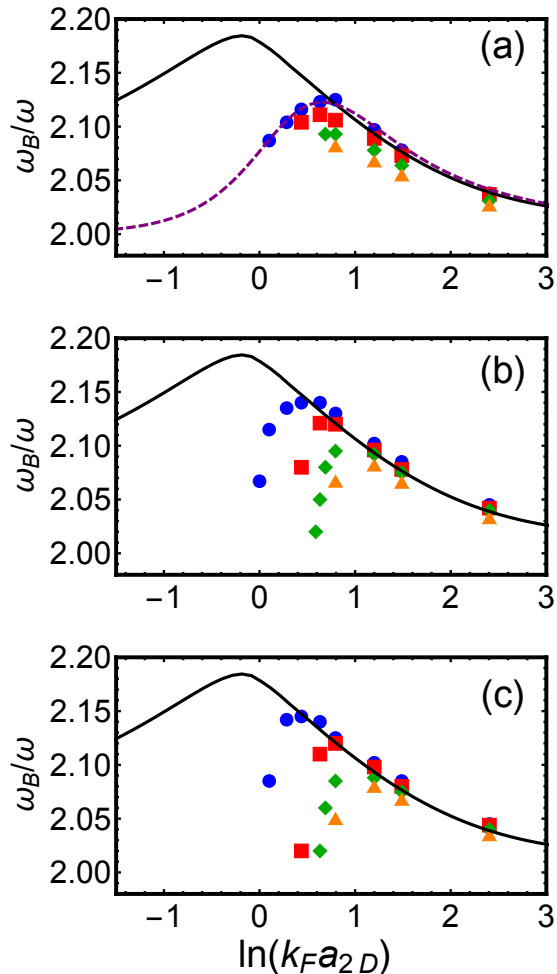


FIG. 2. Symbols in (a), (b), and (c) show the breathing mode frequency ω_B as a function of logarithm of scattering length for (1, 1), (2, 2), and (3, 3) systems, respectively. Blue circles, red squares, green diamonds, and orange triangles are for $k_F^2 R_s = -0.0245, -0.245, -0.620,$ and -0.980 , respectively. The solid line shows the zero-range result in the many-body limit based on AFQMC equation of state while the dashed line shows the exact two-body zero-range solution [33].

$m_p \equiv \int d\omega \omega^p S_{\mathcal{F}}(\omega)$. In harmonic traps, both the energy weighted moments m_1 and m_{-1} can be easily calculated at zero temperature. The former can be transformed into the calculation of commutators involving the operator \mathcal{F} and the Hamiltonian [37], leading to $m_1 \propto \langle r^2 \rangle = \int_0^\infty n(r) r^3 dr$, where $\langle r^2 \rangle$ is the square cloud width calculated using the density distribution $n(r)$. The moment m_{-1} , on the other hand, is proportional to the linear static response of the operator \mathcal{F} , $m_{-1} \propto \partial \langle r^2 \rangle / \partial (\omega^2)$ [37]. Putting the two moments together, we obtain an elegant expression for the breathing

mode frequency [38, 39],

$$\omega_B^2 = -2 \langle r^2 \rangle \left[\frac{\partial \langle r^2 \rangle}{\partial (\omega^2)} \right]^{-1}. \quad (5)$$

The accuracy of the above sum-rule expression may be examined in the many-particle limit, by using alternative two-fluid hydrodynamic theory [40] for the breathing mode frequency in case of zero range interaction. We outline the details in Supplemental Material [33]. For our few-body calculations, which are performed in harmonic oscillator unit, we define $a_{2D} = x a_{\text{ho}}$, $R_s = y a_{\text{ho}}^2$, and $\langle r^2 \rangle = z a_{\text{ho}}^2$, where x , y , and z are dimensionless. If we keep ω a constant while vary a_{2D} and R_s proportionally, i.e., keep y/x^2 a constant, the sum rule result can be alternatively expressed as

$$\omega_B^2 = 4\omega^2 / \left(1 - \frac{x}{2z} \frac{dz}{dx} \right). \quad (6)$$

This allows us to compute ω_B for few-body systems through a finite difference method [33]. To compare ω_B for (1, 1), (2, 2), and (3, 3) systems, and to provide insights for larger systems, we express the harmonic oscillator length a_{ho} in terms of Fermi wavevector k_F and consequently use the dimensionless interaction parameters $\ln(k_F a_{2D})$ and $k_F^2 R_s$.

Symbols in Fig. 2(a), (b), and (c) show the breathing mode frequency ω_B as a function of $\ln(k_F a_{2D})$ for various effective ranges $k_F^2 R_s$, ranging from close to zero to around -1 . The solid line shows the zero-range many-body results determined using the equation of state from auxiliary-field quantum Monte Carlo (AFQMC) [33]. In all regimes, ω_B is greater than the scale invariance value 2ω . It peaks within strongly interacting regime, gradually decreases towards the BCS limit, and decreases sharply towards the BEC limit.

As the effective range $k_F^2 R_s$ approaches zero, our finite-range few-body results approaches the zero-range many-body result. The difference between $k_F^2 R_s = -0.0245$ results, where $k_F^2 R_s$ is very close to zero, and the zero-range many-body result is very small on the BCS side and could likely be attributed to the finite size effect. However, the discrepancy becomes prominent when $\ln(k_F a_{2D}) < 0.2$. This may be caused by the dramatically increased peak density in the strongly interacting regime, where the wavevector k_F of the non-interacting trapped Fermi gas is no longer a proper choice for parameterization. The actual effective range at the trap center is larger, leading to a significant deviation in the breathing mode frequency with respect to the zero-range result. Notably, our numerical result for (1, 1) system with $k_F^2 R_s = -0.0245$ agrees extremely well with the prediction from the exact two-body zero-range solution [33], based on the seminal work of Busch et al. [41].

As $k_F^2 R_s$ increases, the quantum anomaly, i.e., the difference between ω_B and scale invariance value 2ω , is grad-

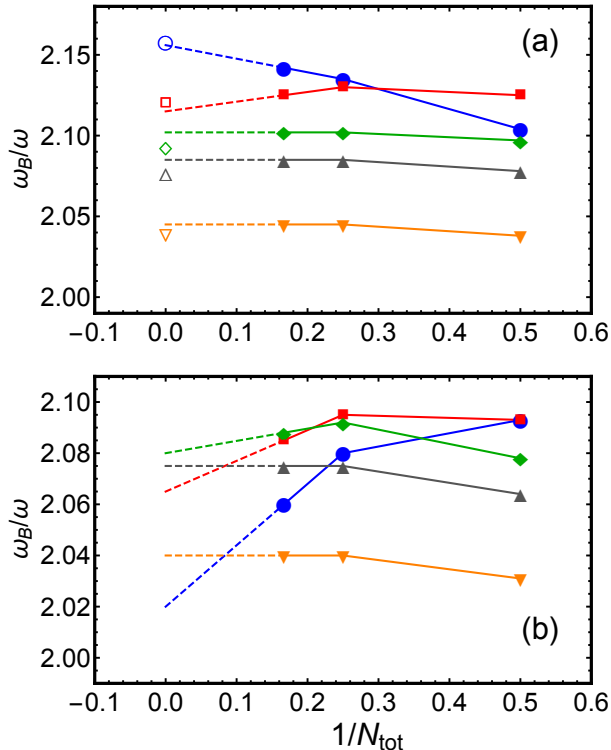


FIG. 3. (a) Circles, squares, diamonds, upper triangles, and lower triangles show the breathing mode frequency ω_B as a function of $1/N_{\text{tot}}$ at $\ln(k_F a_{2D}) = 0.284, 0.794, 1.20, 1.49,$ and 2.40 , respectively. The effective range is $k_F^2 R_s = -0.0245$. The hollow symbols at $1/N_{\text{tot}} = 0$ show the many-body result at zero effective range. (b) Circles, squares, diamonds, upper triangles, and lower triangles show the breathing mode frequency ω_B as a function of $1/N_{\text{tot}}$ at $\ln(k_F a_{2D}) = 0.689, 0.794, 1.20, 1.49,$ and 2.40 , respectively. The effective range is $k_F^2 R_s = -0.620$. In both plots, dashed lines show the linear extrapolation of (2,2) and (3,3) results towards the many-particle limit $N_{\text{tot}} \rightarrow \infty$.

ually suppressed across all scattering strength. Specifically, as $k_F^2 R_s$ increases from near zero to around -1 , the maximum value of breathing mode shift decreases from 7.5% to 4%. Also, the scattering length where maximum value of ω_B occurs shifts towards the BCS limit as $k_F^2 R_s$ increases. The downward shifting of ω_B as the effective range increases qualitatively agrees with the trend observed in the many-body calculations [13, 14].

Although we consider only (1,1), (2,2), and (3,3) systems, it is important to analyze the finite size effects and the trend as the system size increases. This will allow us to see how our few-body results connect to the many-body limit. Solid symbols in Fig. 3(a) show ω_B as a function of $1/N_{\text{tot}}$ for $k_F^2 R_s = -0.0245$ and different values of $\ln(k_F a_{2D})$ across the BEC-BCS crossover. Overall, the differences between the (2,2) and (3,3) systems are very small. Since (1,1) system cannot capture the many-body

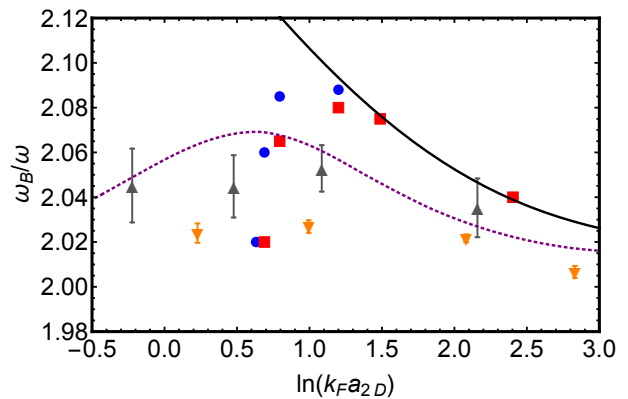


FIG. 4. Circles and squares show the breathing mode frequency ω_B as a function of $\ln(k_F a_{2D})$ for (3,3) system and for the extrapolated many-body result, respectively. The effective range is fixed to $k_F^2 R_s = -0.620$. Upper and lower triangles show the experimental data by Peppler *et al.* (Swinburne) [11] and Holten *et al.* (Heidelberg) [10]. The solid line shows the zero-range AFQMC result in the many-body limit while the dotted line shows the latest many-body result [14].

correlations beyond two-body level, it is expected to see a significant difference between (1,1) system and larger systems. If we do a simple linear extrapolation of (2,2) and (3,3) results towards the $1/N_{\text{tot}} = 0$ limit [42], the extrapolated results agree reasonably well with the many-body AFQMC result shown in hollow symbols. The good agreement encourages us to perform the same extrapolation for the data with effective range $k_F^2 R_s = -0.620$, which is the realistic effective range in recent two ${}^6\text{Li}$ experiments [10, 11, 13]. This is shown in Fig. 3(b) by dashed lines. From the results at zero-range, we estimate that the systematic error in the extrapolated mode frequency due to our naive extrapolation procedure is about $(0.01 - 0.02)\omega$.

Comparison with experiments. — The main motivation for this work is the discrepancy between the large quantum anomaly ($\sim 10\%$) predicted with zero-range model and the much smaller quantum anomaly ($< 3\%$) observed in the experiments [10, 11]. In both Heidelberg and Swinburne experiments, two hyperfine states of ${}^6\text{Li}$ are cooled to deep quantum degeneracy in a 2D trap. It has been shown that the effective range in those setups are non-negligible [13]. Here, we compare the experimental data with our few-body results with same value of $k_F^2 R_s = -0.620$ in Fig. 4. Circles and squares show the (3,3) system results and extrapolated many-body results following Fig. 3(b). Upper and lower triangles show the experimental data from Swinburne and Heidelberg groups [10, 11], respectively.

Although we have observed a reduced quantum anomaly with finite effective range, quantitative discrepancy between experimental data and our few-body results exist. One of the reasons could be the residual

finite temperature effect. The temperature in both experiments is at the range of $(0.1 - 0.2)T_F$, where T_F is Fermi temperature. It has been shown that the quantum anomaly is reduced at non-zero temperature [9]. Combining the finite range effect and the finite temperature effect, we expect that the quantum anomaly should be further reduced. These two effects together, could possibly explain the much smaller deviation observed in the experiments [10, 11].

Conclusions. — We have calculated the breathing mode frequency of a two-component Fermi cloud with a few particles up to six in two dimensions. We have found that the quantum anomaly, i.e., the enhancement of the breathing mode frequency with respect to its classical scale invariant value, is gradually suppressed as effective range of interactions increases. In particular, the maximum value of the breathing mode frequency is reduced while the interaction strength corresponding to the maximum value shifts towards the weak-coupling limit. These two key trends qualitatively agree with recent experiments. Our accurate few-body results open a new way to better understand the intriguing quantum anomaly and provide benchmark predictions for future few-particle experiments in microtraps and optical tweezers.

We are grateful for discussions with Jia Wang. This research was supported by the Australian Research Council (ARC) Discovery Programs, Grants No. DP170104008 (H.H.), No. FT140100003 (X.-J.L) and No. DP180102018 (X.-J.L).

-
- [1] L. P. Pitaevskii and A. Rosch, Breathing modes and hidden symmetry of trapped atoms in two dimensions, *Phys. Rev. A* **55**, R853 (1997).
- [2] M. Olshanii, H. Perrin, and V. Lorent, Example of a Quantum Anomaly in the Physics of Ultracold Gases, *Phys. Rev. Lett.* **105**, 095302 (2010).
- [3] F. Werner and Y. Castin, Unitary gas in an isotropic harmonic trap: Symmetry properties and applications, *Phys. Rev. A* **74**, 053604 (2006).
- [4] J. Hofmann, Quantum Anomaly, Universal Relations, and Breathing Mode of a Two-Dimensional Fermi Gas, *Phys. Rev. Lett.* **108**, 185303 (2012).
- [5] E. Taylor and M. Randeria, Apparent Low-Energy Scale Invariance in Two-Dimensional Fermi Gases, *Phys. Rev. Lett.* **109**, 135301 (2012).
- [6] P. A. Murthy, N. Defenu, L. Bayha, M. Holten, P. M. Preiss, T. Enss, and S. Jochim, Quantum scale anomaly and spatial coherence in a 2D Fermi superfluid, arXiv:1805.04734.
- [7] E. Vogt, M. Feld, B. Fröhlich, D. Pertot, M. Koschorreck, and M. Köhl, Scale Invariance and Viscosity of a Two-Dimensional Fermi Gas, *Phys. Rev. Lett.* **108**, 070404 (2012).
- [8] C. Chafin and T. Schäfer, Scale breaking and fluid dynamics in a dilute two-dimensional Fermi gas, *Phys. Rev. A* **88**, 043636 (2013).
- [9] B. C. Mulkerin, X.-J. Liu, and H. Hu, Collective modes of a two-dimensional Fermi gas at finite temperature, *Phys. Rev. A* **97**, 053612 (2018).
- [10] M. Holten, L. Bayha, A. C. Klein, P. A. Murthy, P. M. Preiss, and S. Jochim, Anomalous Breaking of Scale Invariance in a Two-Dimensional Fermi Gas, *Phys. Rev. Lett.* **121**, 120401 (2018).
- [11] T. Peppler, P. Dyke, M. Zamorano, S. Hoinka, and C. J. Vale, Quantum Anomaly and 2D-3D Crossover in Strongly Interacting Fermi Gases, *Phys. Rev. Lett.* **121**, 120402 (2018).
- [12] D. S. Petrov and G. V. Shlyapnikov, Interatomic collisions in a tightly confined Bose gas, *Phys. Rev. A* **64**, 012706 (2001).
- [13] H. Hu, B. C. Mulkerin, U. Toniolo, L. He, and X.-J. Liu, Reduced Quantum Anomaly in a Quasi-Two-Dimensional Fermi Superfluid: Significance of the Confinement-Induced Effective Range of Interactions, *Phys. Rev. Lett.* **122**, 070401 (2019).
- [14] F. Wu, J. Hu, L. He, X.-J. Liu, and H. Hu, Effective theory for ultracold strongly interacting fermionic atoms in two dimensions, arXiv:1906.08578 (2019).
- [15] A. V. Turlapov and M. Y. Kagan, Fermi-to-Bose crossover in a trapped quasi-2D gas of fermionic atoms, *J. Phys.: Condens. Matter* **29**, 383004 (2017).
- [16] H. Shi, S. Chiesa, and S. Zhang, Ground-state properties of strongly interacting Fermi gases in two dimensions, *Phys. Rev. A* **92**, 033603 (2015).
- [17] E. R. Anderson and J. E. Drut, Pressure, Compressibility, and Contact of the Two-Dimensional Attractive Fermi Gas, *Phys. Rev. Lett.* **115**, 115301 (2015).
- [18] L. M. Schonenberg, P. C. Verpoort, and G. J. Conduit, Effective-range dependence of two-dimensional Fermi gases, *Phys. Rev. A* **96**, 023619 (2017).
- [19] Y. Suzuki and K. Varga, *Stochastic Variational Approach to Quantum-Mechanical Few-Body Problems* (Springer, Berlin, 1998).
- [20] J. Mitroy, S. Bubin, W. Horiuchi, Y. Suzuki, L. Adamowicz, W. Cencek, K. Szalewicz, J. Komasa, D. Blume, and K. Varga, Theory and application of explicitly correlated Gaussians, *Rev. Mod. Phys.* **85**, 693 (2013).
- [21] X.-J. Liu, H. Hu, and P. D. Drummond, Virial Expansion for a Strongly Correlated Fermi Gas, *Phys. Rev. Lett.* **102**, 160401 (2009).
- [22] X.-J. Liu, H. Hu, and P. D. Drummond, Exact few-body results for strongly correlated quantum gases in two dimensions, *Phys. Rev. B* **82**, 054524 (2010).
- [23] D. Blume, Few-body physics with ultracold atomic and molecular systems in traps, *Rep. Prog. Phys.* **75**, 046401 (2012).
- [24] X.-J. Liu, Virial expansion for a strongly correlated Fermi system and its application to ultracold atomic Fermi gases, *Phys. Rep.* **524**, 37 (2013).
- [25] J. Bjerlin, S. M. Reimann, and G. M. Bruun, Few-Body Precursor of the Higgs Mode in a Fermi Gas, *Phys. Rev. Lett.* **116**, 155302 (2016).
- [26] J. Levinsen, P. Massignan, S. Endo, and M. M. Parish, Universality of the unitary Fermi gas: a few-body perspective, *J. Phys. B* **50**, 072001 (2017).
- [27] F. Serwane, G. Zurn, T. Lompe, T. B. Ottenstein, A. N. Wenz, and S. Jochim, Deterministic Preparation of a Tunable Few-Fermion System, *Science* **332**, 336 (2011).
- [28] A. M. Kaufman, B. J. Lester, and C. A. Regal, Cooling a Single Atom in an Optical Tweezer to Its Quantum

- Ground State, Phys. Rev. X **2**, 041014 (2012).
- [29] L. R. Liu, J. D. Hood, Y. Yu, J. T. Zhang, N. R. Hutzler, T. Rosenband, and K.-K. Ni, Building one molecule from a reservoir of two atoms, Science **360**, 900 (2018).
- [30] B. J. Verhaar, J. P. H. W. van den Eijnde, M. A. J. Voermans, and M. M. J. Schaffrath, Scattering length and effective range in two dimensions: application to adsorbed hydrogen atoms, J. Phys. A **17**, 595 (1984).
- [31] S. K. Adhikari, W. G. Gibson, and T. K. Lim, Effective-range theory in two dimensions, J. Chem. Phys. **85**, 5580 (1986).
- [32] Note that the definition of scattering length and effective range in 2D varies in literature. In our choice, R_s has dimension of $length^2$.
- [33] See Supplemental Material at <http://link.aps.org/supplemental/xxxx> for the details of our numerical approach, breathing mode from two-fluid hydrodynamic theory and exact two-body solution, universality and effects beyond effective range, few-body results of the density distribution, and alternative extrapolation to the many-body limit.
- [34] D. Blume and K. M. Daily, Universal relations for a trapped four-fermion system with arbitrary s -wave scattering length, Phys. Rev. A **80**, 053626 (2009).
- [35] D. Blume and K. M. Daily, Trapped two-component Fermi gases with up to six particles: Energetics, structural properties, and molecular condensate fraction, Comptes Rendus Physique **12**, 86 (2011).
- [36] X. Y. Yin and D. Blume, Trapped unitary two-component Fermi gases with up to ten particles, Phys. Rev. A **92**, 013608 (2015).
- [37] F. Dalfovo, S. Giorgini, L. P. Pitaevskii, and S. Stringari, Theory of Bose-Einstein condensation in trapped gases, Rev. Mod. Phys. **71**, 463 (1999).
- [38] C. Menotti and S. Stringari, Collective oscillations of a one-dimensional trapped Bose-Einstein gas, Phys. Rev. A **66**, 043610 (2002).
- [39] H. Hu, G. Xianlong, and X.-J. Liu, Collective modes of a one-dimensional trapped atomic Bose gas at finite temperatures, Phys. Rev. A **90**, 013622 (2014).
- [40] E. Taylor, H. Hu, X.-J. Liu, L. P. Pitaevskii, A. Griffin, and S. Stringari, First and second sound in a strongly interacting Fermi gas, Phys. Rev. A **80**, 053601 (2009).
- [41] T. Busch, B. G. Englert, K. Rzazewski, and M. Wilken, Two Cold Atoms in a Harmonic Trap, Found. Phys. **28**, 549 (1998).
- [42] Alternative extroplation to the many-body limit considering the closed-shell effect is given in Supplemental Material [33].

Supplemental Material for “Few-body perspective of quantum anomaly in two-dimensional Fermi gases”

X. Y. Yin,¹ Hui Hu,¹ and Xia-Ji Liu¹

¹Centre for Quantum and Optical Science, Swinburne University of Technology, Melbourne, Victoria 3122, Australia

I. EXPLICITLY CORRELATED GAUSSIAN TECHNIQUE AND FINITE DIFFERENCE METHOD

To numerically solve the Schrödinger equation for the Hamiltonian given in Eq. (3), we employ explicitly correlated Gaussian (ECG) technique detailed in Ref. [1, 2]. First, we separate off the center of mass degrees of freedom and expand the eigenstates of the relative Hamiltonian in terms of ECG basis functions, which depend on a set of non-linear variational parameters that are optimized through energy minimization. Because the interaction we use is rotational invariant, different angular momentum channels with different m quantum number do not couple, we focus on $m = 0$ channel here. The unsymmetrized basis functions for states with $m = 0$ quantum number read $\exp(-\frac{1}{2}\vec{x}^T A \vec{x})$, where A is a symmetric and positive definite $(N-1) \times (N-1)$ parameter matrix. $\vec{x} = (\vec{x}_1, \vec{x}_2, \dots, \vec{x}_{N-1})^T$ collectively denotes a set of $N-1$ Jacobi vectors. We choose the Jacobi vectors in the same way as detailed in Ref. [3]. A key advantage of these basis functions is that the corresponding overlap and Hamiltonian matrix elements can be calculated analytically [2]. The fermionic exchange symmetry is ensured by acting with the permutation operator on the unsymmetrized basis functions.

We use a stochastic variational approach to choose and optimize the variational parameters contained in A . We start with just one basis function and enlarge the basis set one basis function at a time, which is chosen from 500 trial basis functions. To decide which trial basis function to keep, we calculate the energy for each of the enlarged trial basis sets and choose the one that results in the largest reduction of ground state energy. The procedure is repeated till the basis set is sufficiently complete. After the basis set enlargement process, we then readjust each basis function to further lower the energy. A reoptimization cycle denotes the adjustment process of every basis functions. Typically, 5 complete reoptimization cycles is needed to reach desired accuracy for ground state energy.

As we explained in the main text, breathing mode frequency ω_B can be calculated through Eq. (6). To compute ω_B through finite difference method, we choose two sets of parameters (x_1, y_1) and (x_2, y_2) that satisfy $x_2 = 1.02x_1$ and $y_2 = 1.02^2y_1$. Each set of parameter corresponds to a potential with a certain V_0 and r_0 . Since the parameters for the two potentials are extremely close, we average the two sets of V_0 and r_0 and construct the

basis set according to the averaged potential through the aforementioned basis set enlargement process and 5 complete reoptimization cycles. We then compute z_1 and z_2 using the same basis set. The breathing mode frequency is given by

$$\omega_B^2 = 4\omega^2 / \left(1 - \frac{1}{2} \frac{z_2/z_1 - 1}{x_2/x_1 - 1} \right). \quad (\text{S1})$$

For (1,1) and (2,2) systems, we alternatively compute z_1 and z_2 by constructing two basis sets separately and find good agreement with using the same basis set. Our approach to compute z_1 and z_2 using the same basis set allows for a much faster convergence of ω_B , especially for the (3,3) systems.

While the variational principle guarantees that the ground state energy obtained is a variational upper bound. The same is not true for ω_B . It is therefore much more challenging to estimate the error bar for ω_B . Following the spirit of Ref. [3], we estimate the error bar from the change of ω_B within last 3 reoptimization cycles. Under this assumption, the error bar for (1,1), (2,2), and (3,3) systems are estimated to be $\Delta\omega_B/\omega = \pm 0.0005$, ± 0.002 , and ± 0.008 , respectively.

II. BREATHING MODE FREQUENCY FROM THE TWO-FLUID HYDRODYNAMIC THEORY

In the case of zero-range interaction, we have the accurate zero-temperature equation of state provided by auxiliary-field quantum Monte Carlo (AFQMC) [4]. In the presence of the harmonic trap $V_{ext}(r) = m\omega^2 r^2/2$, the density distribution $n(r)$ can then be determined using the standard local density approximation (LDA) [5]. In addition to the sum-rule approach, we can use the coupled two-fluid hydrodynamic equations to calculate the breathing mode frequency [6]. The normal modes of those equations at frequency Ω are most easily obtained by minimizing a variational action, which, in terms of the displacement field $\mathbf{u}(\vec{r})$, takes the following form [6],

$$\mathcal{S} = \frac{1}{2} \int d\vec{r} \left[m\Omega^2 n \mathbf{u}^2 + 2n (\nabla \cdot \mathbf{u}) (\nabla V_{ext} \cdot \mathbf{u}) + (\nabla n \cdot \mathbf{u}) (\nabla V_{ext} \cdot \mathbf{u}) - n \left(\frac{\partial P}{\partial n} \right) (\nabla \cdot \mathbf{u})^2 \right], \quad (\text{S2})$$

where $[\partial P/\partial n](r)$ is the derivative of the local pressure at position \vec{r} with respect to the local density. For compressional modes (including the lowest breathing mode

of interest), we assume the following polynomial ansatz for the displacement field:

$$\mathbf{u}(r) = \vec{r} \sum_{i=0}^{N_p-1} A_i r^i, \quad (\text{S3})$$

where $\{A_i\}$ ($i = 0, \dots, N_p - 1$) are the N_p variational parameters. By inserting this variational ansatz into the action Eq. (S2), we express the action \mathcal{S} as functions of the N_p variational parameters $\{A_i\}$. The mode frequencies Ω of the N_p compressional modes can then be obtained by minimizing the action \mathcal{S} with respect to the N_p parameters. The accuracy of our variational calculations for the breathing mode can be improved by increasing the value of N_p and the calculations indeed converge very rapidly as N_p increases.

In more detail, it is straightforward to show that, the expression of the action can be written in a compact form,

$$\mathcal{S} = \frac{1}{2} \Lambda^\dagger \mathcal{S}(\Omega) \Lambda, \quad (\text{S4})$$

where $\Lambda \equiv [A_0, \dots, A_i, \dots, A_{N_p-1}]^T$ and $\mathcal{S}(\Omega)$ is a $N_p \times N_p$ matrix with elements $(i, j = 0, \dots, N_p - 1)$,

$$[\mathcal{S}(\Omega)]_{ij} \equiv M_{ij} \Omega^2 - K_{ij}, \quad (\text{S5})$$

where the weighted mass moments are,

$$M_{ij} = m \int d\vec{r} r^{i+j+2} n(r), \quad (\text{S6})$$

and the spring constants are,

$$K_{ij} = (i+2)(j+2) \int d\vec{r} r^{i+j} \left(n \frac{\partial P}{\partial n} \right) (r). \quad (\text{S7})$$

The minimization of the action \mathcal{S} (which is now in a matrix form) is equivalent to solving $\mathcal{S}(\Omega) \Lambda = 0$.

In Fig. S1, we show the breathing mode frequency predicted by the two-fluid hydrodynamic theory with $N_p = 10$ (empty squares), and compare it with the sum-rule result (solid line). The relative difference between the two-fluid hydrodynamic theory and the sum-rule approach is less than 0.1% and cannot be identified at the scale of the figure.

It is interesting to note that, if we assume a *constant* polytropic index

$$\gamma = \frac{n}{P} \left(\frac{\partial P}{\partial n} \right) - 1, \quad (\text{S8})$$

the variational procedure leads to a breathing mode frequency

$$\omega_B^2 = 2(\gamma + 1)\omega^2. \quad (\text{S9})$$

This can be seen by substituting the relation $n(\partial P/\partial n) = (\gamma + 1)P$ into the spring constants Eq. (S7). Using the

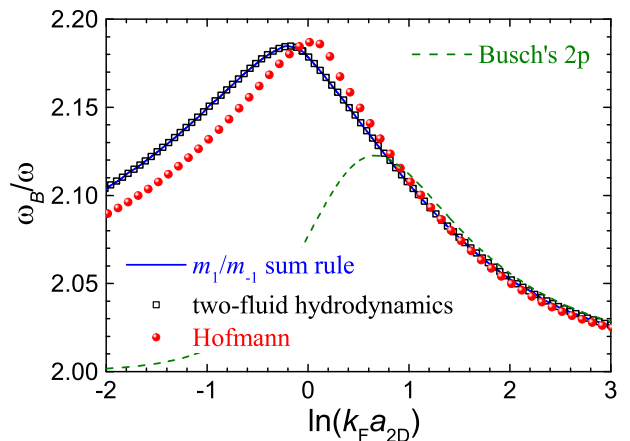


FIG. S1. Breathing mode frequency of a zero-range interacting Fermi gas as a function of $\ln(k_F a_{2D})$, predicted by the sum-rule approach (solid line), Busch's exact two-body solution (dashed line), the two-fluid hydrodynamic theory (open squares) [7], and the simple evaluation adopted by Hofmann (circles) [7]. In all cases, the equation of state simulated by AFQMC is used [4]. The difference between the sum-rule approach and the two-fluid hydrodynamic theory is indistinguishable under the scale of the figure.

force balance condition in harmonic traps, i.e., $\partial P/\partial r = -m\omega^2 r n(r)$, we obtain

$$K_{ij} = M_{ij} \omega^2 \frac{(i+2)(j+2)}{(i+j+2)} (\gamma + 1). \quad (\text{S10})$$

The breathing mode is then decoupled from the other compressional modes, since for either $i = 0$ or $j = 0$, $K_{ij} = 2(\gamma + 1)\omega^2 M_{ij}$. This also gives the mode frequency $\omega_B = \sqrt{2(\gamma + 1)}\omega$. The assumption of a constant polytropic index was used earlier by Hofmann to calculate the quantum anomaly with a zero-range contact interaction [7]. In Fig. S1, we show his results in circles with the updated AFQMC equation of state. In the weak-coupling limit, this simple estimation agrees very well with more accurate predictions from the two-fluid hydrodynamic theory and the sum-rule approach. In the strongly-interacting regime near $\ln(k_F a_{2D}) = 0$, however, there is a small quantitative difference.

III. BREATHING MODE FREQUENCY FROM BUSCH'S EXACT TWO-BODY SOLUTION

For two particles interacting through a zero-range contact potential, we may also calculate the breathing mode frequency using Busch's exact two-body solution [8], which states that the relative wave-function of the two particles (for $\vec{\rho} = \vec{r}_1 - \vec{r}_2$) is given by [8, 9],

$$\psi_{\text{rel}}(\rho) \propto \exp\left(-\frac{\rho^2}{4a_{\text{ho}}^2}\right) \Gamma(-\nu) U\left(-\nu, 1, \frac{\rho^2}{2a_{\text{ho}}^2}\right), \quad (\text{S11})$$

where Γ is the gamma function and U is the second kind of Kummer function. The parameter ν is related to the relative energy $E_{\text{rel}} = (2\nu + 1)\hbar\omega$, and is determined by

$$\gamma - \frac{1}{2}\ln 2 + \frac{1}{2}\psi(-\nu) = \ln\left(\frac{a_{\text{ho}}}{a_{2D}}\right), \quad (\text{S12})$$

where $\gamma \simeq 0.577216$ is the Euler constant and $\psi(x)$ is the digamma function. For the ground state, we have $\nu < 0$. Adding the ground-state center-of-mass wavefunction (for $\vec{R} = (\vec{r}_1 + \vec{r}_2)/2$),

$$\psi_{\text{cm}}(R) \propto \exp\left(-\frac{R^2}{a_{\text{ho}}^2}\right), \quad (\text{S13})$$

we therefore obtain that the total ground-state wavefunction,

$$\Psi_{\text{gs}}(\vec{R}, \vec{\rho}) \propto e^{-\frac{R^2}{a_{\text{ho}}^2}} e^{-\frac{\rho^2}{4a_{\text{ho}}^2}} \Gamma(-\nu) U\left(-\nu, 1, \frac{\rho^2}{2a_{\text{ho}}^2}\right). \quad (\text{S14})$$

It is now straightforward to calculate the square cloud width, which takes the form,

$$\langle r^2 \rangle = \frac{\int d\vec{R}d\vec{\rho} (R^2 + \rho^2/4) \left[\Psi_{\text{gs}}(\vec{R}, \vec{\rho})\right]^2}{\int d\vec{R}d\vec{\rho} \left[\Psi_{\text{gs}}(\vec{R}, \vec{\rho})\right]^2}. \quad (\text{S15})$$

Here we have used the identity $(r_1^2 + r_2^2)/2 = R^2 + \rho^2/4$. By using the dimensionless variables $y = R^2/(2a_{\text{ho}}^2)$ and $x = \rho^2/(2a_{\text{ho}}^2)$, we may write $\langle r^2 \rangle$ into the form,

$$\langle r^2 \rangle = \frac{a_{\text{ho}}^2}{2} \mathcal{F}(\nu), \quad (\text{S16})$$

where the dimensionless function is defined by,

$$\mathcal{F}(\nu) = \frac{\int dy dx (4y + x) e^{-4y} e^{-x} \Gamma^2(-\nu) U^2(-\nu, 1, x)}{\int dy dx e^{-4y} e^{-x} \Gamma^2(-\nu) U^2(-\nu, 1, x)}.$$

The integration over the variable y can be easily done and we obtain

$$\mathcal{F}(\nu) = \frac{\int dx (1+x) e^{-x} \Gamma^2(-\nu) U^2(-\nu, 1, x)}{\int dx e^{-x} \Gamma^2(-\nu) U^2(-\nu, 1, x)}.$$

We then write $\mathcal{F}(\nu) = 1 + B_\nu/A_\nu$, where

$$A_\nu = \int dx e^{-x} \Gamma^2(-\nu) U^2(-\nu, 1, x),$$

$$B_\nu = \int dx x e^{-x} \Gamma^2(-\nu) U^2(-\nu, 1, x).$$

To finish the integral on the variable x , we can use the identity

$$\Gamma(-\nu) U(-\nu, 1, x) = \sum_{k=0}^{\infty} \frac{L_k(x)}{k-\nu} \quad (\text{S17})$$

to obtain

$$A_\nu = \sum_{n=0}^{\infty} \frac{1}{(n-\nu)^2},$$

$$B_\nu = \sum_{n=0}^{\infty} \frac{1}{n-\nu} \left[\frac{1+2\nu}{n-\nu} - \frac{1+\nu}{n-\nu-1} - \frac{\nu}{n-\nu+1} \right].$$

Here, $L_k(x)$ is Laguerre polynomial, satisfying,

$$\int_0^\infty dx e^{-x} L_m(x) L_n(x) = \delta_{mn},$$

and

$$(k+1)L_{k+1}(x) = (2k+1-x)L_k(x) - kL_{k-1}(x).$$

We can now use the f -sum rule

$$\frac{\omega_B^2}{\omega^2} = -2 \frac{\langle r^2 \rangle}{\omega^2 \left[\frac{\partial \langle r^2 \rangle}{\partial (\omega^2)} \right]} \quad (\text{S18})$$

to calculate the breathing mode frequency. By noting that $a_{\text{ho}}^2 \propto \omega^{-1}$ and $a_{\text{ho}}/a_{2D} \propto (\omega^2)^{-1/4}$, it is easy to show that,

$$\frac{\omega_B^2}{\omega^2} = 4 \left[1 + \frac{1}{2} \frac{\partial \ln \mathcal{F}}{\partial \ln (a_{\text{ho}}/a_{2D})} \right]^{-1}. \quad (\text{S19})$$

For two particles, the Fermi wavevector k_F is given by, $k_F = 2^{3/4} a_{\text{ho}}^{-1}$. Therefore, we have the relation,

$$\ln(k_F a_{2D}) = \frac{3}{4} \ln 2 - \ln \frac{a_{\text{ho}}}{a_{2D}}. \quad (\text{S20})$$

We can further cast the breathing mode frequency into the form,

$$\omega_B = 2\omega \left[1 - \frac{1}{2} \frac{\partial \ln \mathcal{F}}{\partial \ln (k_F a_{2D})} \right]^{-1/2}. \quad (\text{S21})$$

Numerically, for a given $\ln(k_F a_{2D})$, we first calculate ν by using

$$\gamma + \frac{1}{2}\psi(-\nu) = \frac{5}{4} \ln 2 - \ln(k_F a_{2D}), \quad (\text{S22})$$

and then calculate A_ν and B_ν to obtain $\mathcal{F} = (1 + B_\nu/A_\nu)$. This leads to a curve of $\ln \mathcal{F}$ as a function of $\ln(k_F a_{2D})$. We finally take the numerical derivative in Eq. (S21) to obtain the breathing mode frequency.

As shown in Fig. S1, we find that the breathing mode frequency from Busch's exact two-body solution agrees well with the many-body prediction at $\ln(k_F a_{2D}) \gtrsim 0.7$. Once the interaction parameter is smaller than this value, there is a significant difference, as the many-body correlation starts to make a dominant contribution to the breathing mode. In the main text, we show that the exact two-body solution agrees very well with the numerical results for (1, 1) system with the smallest effective range.

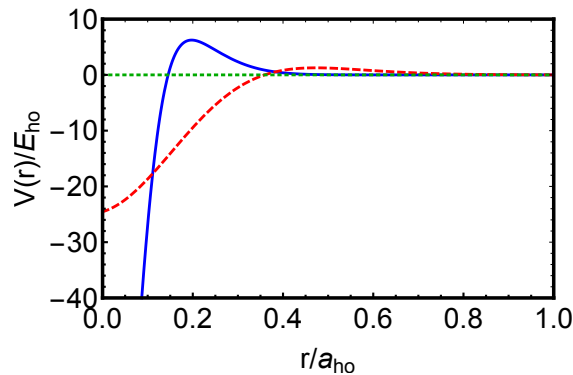


FIG. S2. Solid line shows pseudopotential $V(r)$ at $V_0/E_{\text{ho}} = -120.934$ and $r_0/a_{\text{ho}} = 0.0641$. Dashed line shows pseudopotential $V_s(r)$ at $V_0/E_{\text{ho}} = -27.7817$ and $r_0/a_{\text{ho}} = 0.1776$. Dotted line marks the line $V(r) = 0$.

IV. UNIVERSALITY AND EFFECTS BEYOND EFFECTIVE RANGE

In the main text, we discussed how breathing mode frequency changes with regard to the scattering length a_{2D} and effective range R_s . Here, we analyze the effects beyond the effective range contribution. In addition to the potential, Eq. (4), considered in the main text, we additionally consider a different potential

$$V_s(r) = V_0 \exp\left(-\frac{r^2}{2r_0^2}\right) - V_0 \frac{r}{a_{\text{ho}}} \exp\left[-\frac{r^2}{(2r_0)^2}\right]. \quad (\text{S23})$$

Note that, the potential $V(r)$, Eq. (4), can produce a much larger range of a_{2D} and R_s for negative R_s than $V_s(r)$. Therefore, we are only able to compare the results from the two different potentials for limited data points.

First, we adjust V_0 and r_0 in both potentials and plot them in Fig. S2, such that the scattering length and effective range are $a_{2D} = 2.213a_{\text{ho}}$ and $R_s = -0.0612a_{\text{ho}}^2$, respectively. For $(2, 2)$ system, this corresponds to $k_F a_{2D} = 1.488$ and $k_F^2 R_s = -0.245$. It shows that potential $V_s(r)$ has a much smaller barrier while extends to a longer range. Our calculation shows that the breathing mode frequency ω_B are 2.078ω and 2.075ω , respectively, for $V(r)$ and $V_s(r)$, where the difference is around 0.15%. It's worth noting that the ground state energies are $2.433E_{\text{ho}}$ and $2.464E_{\text{ho}}$, respectively, where the difference is 1.2%. This shows that the beyond effective range contribution to breathing mode frequency is indeed negligible.

Second, we repeat the comparison for two additional data points in $(2, 2)$ system. For $k_F a_{2D} = 1.488$ and $k_F^2 R_s = -0.0245$, ω_B are 2.085ω and 2.080ω , respectively, for $V(r)$ and $V_s(r)$. For $k_F a_{2D} = 1.120$ and $k_F^2 R_s = -0.0245$, ω_B are 2.102ω and 2.095ω , respectively, for $V(r)$ and $V_s(r)$. By comparing three sets of data points, we confirm the trend that effective range reduces quantum anomaly is valid for a different potential.

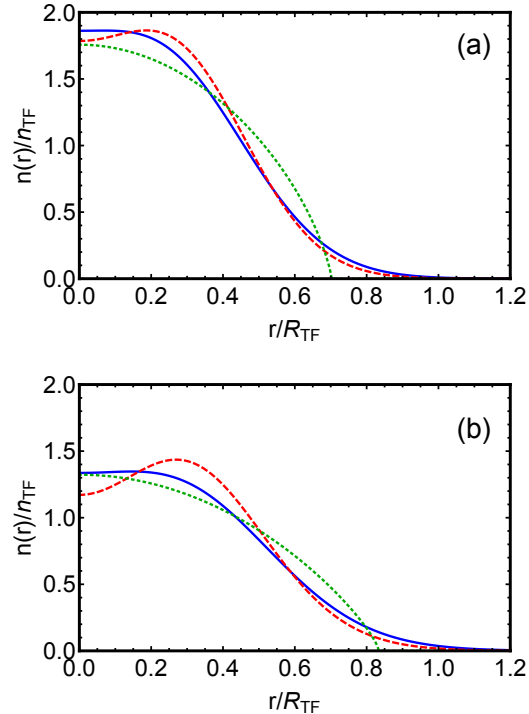


FIG. S3. Solid [dashed] lines in (a) and (b) show the normalized density distribution $n(r)/n_{\text{TF}}$ of $(2, 2)$ [(3, 3)] systems for $\ln(k_F a_{2D}) = 0.101$ and 1.490 . The effective range is $k_F^2 R_s = -0.0245$. Dotted lines show the local density approximation results for the same $\ln(k_F a_{2D})$, calculated based on the AFQMC equation of state with a zero-range interaction [4].

This also suggests that beyond effective range contribution to breathing mode frequency is small to negligible.

V. FEW-BODY RESULTS ON THE DENSITY PROFILE

As we mentioned earlier, the agreement between our few-body results and many-body AFQMC results for breathing mode frequency becomes worse when $\ln(k_F a_{2D}) < 0.2$. The reason is that the Fermi wave vector $k_F = \sqrt{2}(N_{\text{tot}})^{1/4} a_{\text{ho}}^{-1}$ for a trapped two-component Fermi gas is defined at the non-interacting limit. When $\ln(k_F a_{2D})$ approaches zero, the interaction becomes stronger and deeper two-body bound state starts to form. In this regime, the density distribution $n(r)$ becomes very different from that of non-interacting Fermi gas $n_0(r)$.

Figure S3(a) and (b) show the density distribution at $\ln(k_F a_{2D}) = 0.101$ and 1.490 , respectively. The density is normalized by Thomas-Fermi density $n_{\text{TF}} = (\sqrt{N_{\text{tot}}}/\pi) a_{\text{ho}}^{-2}$ while the radius is normalized by Thomas-Fermi radius $R_{\text{TF}} = (4N_{\text{tot}})^{1/4} a_{\text{ho}}$. Solid and dashed lines show the few-body $(2, 2)$ and $(3, 3)$ results while

VI. ALTERNATIVE EXTRAPOLATION TO THE MANY-BODY LIMIT

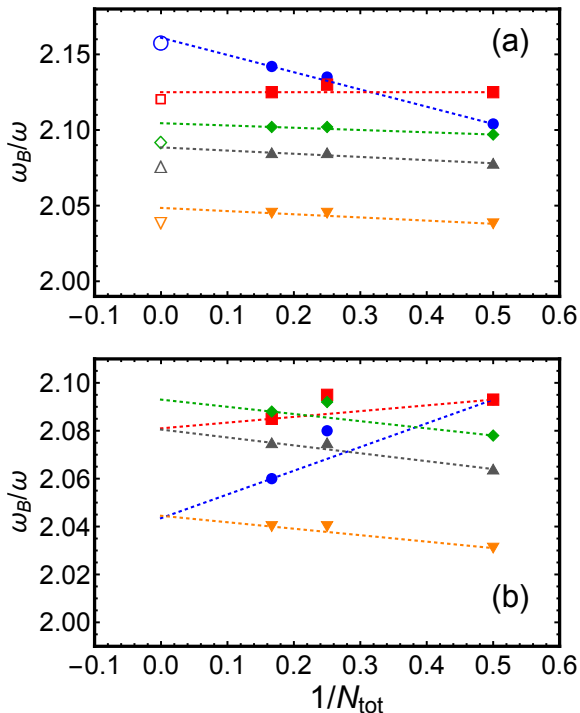


FIG. S4. Same as Fig.3 in the main text, except that dotted lines show the linear extrapolation of (1,1) and (3,3) results towards the many-particle limit $N_{\text{tot}} \rightarrow \infty$.

the dotted lines show the LDA results based on the AFQMC equation of state. These are to be compared with the non-interacting density distribution $n_0(r) = n_{\text{TF}}(1 - r^2/R_{\text{TF}}^2)\Theta(R_{\text{TF}} - r)$. In both few-body and LDA results, the peak density at strongly interacting regime is much higher than the non-interacting limit, and approaches two times the Thomas-Fermi density when $\ln(k_F a_{2D})$ goes to zero. In this regime, k_F is no longer an appropriate unit to characterize the few-body and many-body results.

In the main text, we discussed a naïve extrapolation from few-body results to the many-body limit $N_{\text{tot}} \rightarrow \infty$. An argument can be made that both (1,1) and (3,3) systems are closed-shell [10]. Therefore, it is worthwhile to show an alternative extrapolation from (1,1) and (3,3) results in Fig. S4. The difference between the two sets of extrapolated results are at most 1%.

- [1] J. Mitroy, S. Bubin, W. Horiuchi, Y. Suzuki, L. Adamowicz, W. Cencek, K. Szalewicz, J. Komasa, D. Blume, and K. Varga, Theory and application of explicitly correlated Gaussians, *Rev. Mod. Phys.* **85**, 693 (2013).
- [2] Y. Suzuki and K. Varga, *Stochastic Variational Approach to Quantum-Mechanical Few-Body Problems* (Springer, Berlin, 1998).
- [3] X. Y. Yin and D. Blume, Trapped unitary two-component Fermi gases with up to ten particles, *Phys. Rev. A* **92**, 013608 (2015).
- [4] H. Shi, S. Chiesa, and S. Zhang, Ground-state properties of strongly interacting Fermi gases in two dimensions, *Phys. Rev. A* **92**, 033603 (2015).
- [5] F. Dalfovo, S. Giorgini, L. P. Pitaevskii, and S. Stringari, Theory of Bose-Einstein condensation in trapped gases, *Rev. Mod. Phys.* **71**, 463 (1999).
- [6] E. Taylor, H. Hu, X.-J. Liu, L. P. Pitaevskii, A. Griffin, and S. Stringari, First and second sound in a strongly interacting Fermi gas, *Phys. Rev. A* **80**, 053601 (2009).
- [7] J. Hofmann, Quantum Anomaly, Universal Relations, and Breathing Mode of a Two-Dimensional Fermi Gas, *Phys. Rev. Lett.* **108**, 185303 (2012).
- [8] T. Busch, B. G. Englert, K. Rzazewski, and M. Wilken, Two Cold Atoms in a Harmonic Trap, *Found. Phys.* **28**, 549 (1998).
- [9] X.-J. Liu, H. Hu, and P. D. Drummond, Exact few-body results for strongly correlated quantum gases in two dimensions, *Phys. Rev. B* **82**, 054524 (2010).
- [10] J. Bjerlin, S. M. Reimann, and G. M. Bruun, Few-Body Precursor of the Higgs Mode in a Fermi Gas, *Phys. Rev. Lett.* **116**, 155302 (2016).